AIAA JOURNAL
Vol. 48, No. 9, September 2010

Nonlinear Analysis of Smart Composite Plates Including Hysteresis Effects

V. L. Sateesh,* C. S. Upadhyay,† and C. Venkatesan‡
Indian Institute of Technology, Kanpur 208016, India

DOI: 10.2514/1.J050223

The coupled electrothermoelastic constitutive relations, representing the behavior of piezo materials, are shown to be nonlinear when the polarization–electric field interaction effects are properly accounted for. Under static condition, the polarization–electric field nonlinearities correspond to a distributed body force and body moment. For time varying situations, polarization–electric field interaction exhibits a hysteresis effect. Using the nonlinear constitutive relations, a layer-by-layer finite element formulation is developed for both static and dynamic analyses of smart plates including hysteresis effects. Linear and nonlinear analyses are carried out to study the effect of nonlinearity due to polarization–electric field interaction on the response of the smart plates. To validate the present formulation, the results of static analysis of a smart plate are compared with experimental data available in literature. It is observed that the *P-E* hysteresis effects show a friction-type damping in the dynamic response of the smart plate.

Nomenclature

b_{ij}	=	electric susceptibility
C_{ijkl}	=	elastic constants
C_θ	=	thermal constant
D	=	electric displacement
dS	=	elemental surface area
dV	=	elemental volume
e_{klm}	=	piezoelectric constants
E	=	electric field
E_C	=	coercive electric field
$E_{C\max}$	=	coercive electric filed corresponding to saturation polarization
$\tilde{F}$	=	modal force vector
f_i	=	body force terms
G	=	shear modulus
H	=	thickness of the plate
H_{ijklm}, Q_{ijkl}	=	real constants
$[K]^L$	=	linear stiffness matrix
$[K_1]$	=	stiffness matrix due to nonlinear force
$[K_2]$	=	stiffness matrix due to nonlinear couple
$[K_3]$	=	stiffness due to higher order terms in constitutive relations
L_1, L_2	=	in-plane dimensions of the plate
$[M]$	=	mass matrix
$\bar{M}_j$	=	out-of-plane basis functions
N_i	=	in-plane shape functions
$\mathbf{n}$	=	unit normal vector
P	=	polarization
$\{q\}$	=	displacement vector $\{u, v, w, \phi, \Theta\}^T$
S	=	length-to-thickness ratio of the plate
T	=	surface traction
$\{U\}$	=	mechanical displacement vector ($\{u, v, w\}^T$)
u_{ij}, v_{ij}, and w_{ij}	=	nodal degrees of freedom along x, y and z axes, respectively
u and v	=	in-plane displacements along x and y axes, respectively
w	=	out-of-plane displacement along z-axis
$\{x\}$	=	displacement vector $\{u, v, w, \phi\}$
α_{ij}	=	thermoelastic constant
β_i	=	constant
Γ_i	=	constants
$\delta()$	=	variation
ϵ_i^s	=	permittivity of material
ϵ_{ij}	=	strain
$\eta(t)$	=	generalized coordinates
Θ	=	internal variable
λ_k	=	pyroelectric constants
ξ, Ω_{ij}, ζ	=	constants
ρ_m	=	mass density
σ^L	=	linear stress tensor
$\sigma_{ij}^{\mathrm{NL}}$	=	antisymmetric part of stress tensor
$[\Phi]$	=	modal matrix
ϕ	=	electric potential
$\{\phi\}^A$	=	applied electric potential
$\{\phi\}^S$	=	induced electric potential
Ψ	=	Helmholtz free energy per unit volume
ω	=	natural frequency
$\dot{()}$	=	double derivative with respect to time

Received 18 September 2009; revision received 4 May 2010; accepted for publication 5 May 2010.

*Graduate Student, Department of Aerospace Engineering.
†Associate Professor, Department of Aerospace Engineering.
‡Pandit Ramachandra Dwivedi Chair Professor, Department of Aerospace Engineering; cven@iitk.ac.in. Senior Member AIAA.

I. Introduction

THE field of smart structures has emerged as an important area of research, particularly from the points of view of sensing and control of structural deformations [1], and health and usage monitoring to establish the useful life of structures [2]. Under external loading, conventional structures have no control over the deformed shape, whereas in smart or intelligent structures the deformation is continuously monitored and controlled by using distributed sensors and actuators. This paper focuses on piezo laminated composite plates and hence the discussion is restricted to piezo materials. These materials, due to the inherent microstructural details, have very interesting temporal response characteristics. These are manifested through the polarization–electric field (*P-E*) hysteresis curve, typical of ferroelectric materials. Piezoelectric materials also demonstrate strain-electric field (ϵ-*E*) hysteresis through a butterfly loop. In [3], it is shown experimentally that strain-electric field relation need not be in the form of butterfly loop at low electric fields. The nonlinear electroelastic formulation developed in this study is shown to predict a similar behavior observed in [3].

With the use of piezo materials in the construction of smart structures, it becomes essential to use a suitable mathematical model representing the electrothermomechanical characteristics of piezo materials. Linear electroelastic constitutive relations for piezoelectric materials have been given by Toupin [4] and Tiersten [5]. However, it was shown in [6,7] that the governing equilibrium equation and the constitutive relationships are inherently nonlinear in nature, due to the polarization–electric field (*P-E*) interaction. The polarization–electric field interaction results in a nonlinear body force term in the force equilibrium equations and also renders the stress tensor nonsymmetric. For dynamic analysis of smart structures, hysteresis effects due to polarization–electric field interaction have to be included.

In the literature, several models have been proposed to capture the *P-E* hysteresis effects at microscopic [8–11] as well as macroscopic [12–14] levels of material medium. Microscopic models are further classified under two categories, namely, models based on phase field simulations [12] and models based on domain switching criteria [9–11]. Macroscopic models can be grouped into empirical models [12] and phenomenological models [13,14]. Microscopic models are difficult to introduce in structural applications, whereas most of the macroscopic models are empirical and do not satisfy the thermodynamic laws. Sateesh et al. [15] have derived the electrothermoelastic constitutive relations for the piezo materials including the hysteresis effects by following fundamental principles of physics.

Crawley and Lazarus [16] have conducted experiments on smart plates containing segmented piezo patches on either side. Four different plate configurations were considered for the experimental study. One plate has aluminum core and the other three plates have composite core with ply orientations $[0/\pm 45]_s$, $[+30_2/0]_s$ and $[+45_3/-45_3]$ respectively. It is shown that the required deformations can be obtained in smart plates by taking advantage of stiffness coupling in substrate.

The static linear analysis of smart plates has been carried out by various researchers for surface mounted as well as embedded piezo patches. Three dimensional analytical solutions of composite plates with surface mounted piezo layers under cylindrical bending have been given by Ray et al. [17] and Heyliger and Brooks [18] for applied traction and electric potential. Simply-supported boundary conditions have been employed for the analysis. It has been concluded that the effectiveness of the actuator layer depends on the length-to-thickness ratio of the substrate. Analytical solutions of laminated piezoelectric plates subjected to applied traction or electric potential have been given by Heyliger [19,20]. Vel and Batra [21] have analyzed composite plates with embedded piezo layers. Vel and Batra have derived the exact solution for a smart composite plate with generalized boundary conditions in [22] and for segmented actuators under cylindrical bending in [23].

Layer-by-layer finite element formulation for laminated composite plates has been developed by Garcao et al. [24]. The analysis has been carried out by using two different interpolation schemes with three different orders of interpolation functions. It has been shown that the through thickness approximation of the displacement plays a major role in the accuracy of the solution. Ha et al. [25] and Saravanos et al. [26] have carried out static and dynamic analysis of cantilever plates with segmented piezo patches by using layer-by-layer finite element modeling. The results of the static analysis have been compared with the experimental data given in [16]. It is observed that the correlation between theoretical and experimental data was found to be better for longitudinal deflection than that observed for lateral bending and twisting. Jin and Batra [27] have used first order shear deformation theory to study the static and dynamic response of plates. The results of the static analysis have been correlated with the experimental data given in [16]. It has been concluded that the longitudinal bending correlated well with the experimental data while the correlation of transverse bending and twisting is not satisfactory.

Heyliger and Saravanos [28] have obtained the natural frequencies for a simply-supported homogeneous piezo plate and composite plates with surface mounted piezo layers using closed form solution. In the dynamic analysis, Ha et al. [25] have analyzed the response of a cantilever plate with distributed piezo patches. Natural frequencies have been obtained experimentally and compared with the numerical results. In [26], Saravanos et al. have obtained the natural frequencies for a composite plate with continuous and multiple piezo patches. Jin and Batra [27] have shown that the difference between the natural frequency of a smart plate with the piezo layers grounded on both top and bottom faces [closed circuit (CC) or short circuit] to that with one face grounded [open circuit (OC)] is about 14%. Kim et al. [29] have modeled smart plates by using three dimensional finite elements. It is shown that the natural frequencies of a cantilever plate, predicted by the proposed model correlate well with the experimental data. David and Touratier [30] have proposed a refined plate theory for static and dynamic analysis of smart plates and validated the results with exact solutions given in [28]. This theory considers quadratic approximation for electric potential and higher order approximation for mechanical displacement field in thickness direction of plate.

In all these studies, nonlinear effects due to polarization–electric field interaction have not been considered. In [31], using a nonlinear formulation Ahmad et al. have analyzed the static deformation of smart beams by layerwise finite element model. It is concluded that the effect of *P-E* nonlinearity is to increase the deflection of the beam for a given actuation voltage. The review of the literature clearly indicates that in the dynamic analysis of smart structural elements, *P-E* hysteresis dissipation loss has not been considered. The objectives of this study are as follows: 1) nonlinear electroelastic formulation for the analysis of smart composite plates, 2) analysis of the variation of strain with respect to time varying electric field, when the electric field is oscillated with varying amplitude of electric field, 3) development of a layerwise finite element formulation for static and dynamic analysis of smart plates including hysteresis effect, and 4) evaluation of the effect of nonlinearities in static and dynamic analysis of smart composite plates.

II. Nonlinear Constitutive Relations and Governing Equations

For obtaining the constitutive relations, the free energy Ψ is expressed as a quadratic function of all state variables and quartic functions of strain and electric field [15]:

$$\begin{aligned}\Psi = \frac{1}{2}\{&C_{ijkl}\epsilon_{kl} - b_{ij}E_iE_j + C_\theta\theta^2 + \xi\Theta^2 - 2e_{ijk}E_i\epsilon_{jk} + 2\alpha_{ij}\epsilon_{ij}\theta \\ &+ 2\lambda_iE_i\theta - 2\Omega_{ij}\epsilon_{ij}\Theta - 2\beta_iE_i\Theta + 2\zeta\Theta\theta - Q_{ijkl}E_iE_jE_kE_l \\ &- H_{ijklm}\epsilon_{ij}E_kE_lE_m + f_{ijklmn}\epsilon_{ij}\epsilon_{kl}E_mE_n - g_{ijklmno}\epsilon_{ij}\epsilon_{kl}\epsilon_{mn}E_o \\ &+ X_{ijklmnop}\epsilon_{ij}\epsilon_{kl}\epsilon_{mn}\epsilon_{op}\}\end{aligned} \tag{1}$$

where C_{ijkl} is the elastic constant, b_{kl} is the electric susceptibility; e_{ijl} is the piezoelectric constant; ξ, β_i Ω_{ij}, ζ, H_{ijklm} and Q_{ijkl} are real constants. The quartic terms in the energy expression Ψ are introduced to properly model the *P-E* hysteresis effects near the saturation polarization. Using the expression for Ψ and by neglecting temperature effects, the set of constitutive relations representing electroelastic process including electric hysteresis effects can be written as [15]

$$\begin{aligned}\sigma_{ij} = &C_{ijkl}\epsilon_{kl} - e_{ijk}E_k - H_{ijklm}E_kE_lE_m - \Omega_{ij}\Theta - P_iE_j \\ &+ f_{ijklmn}\epsilon_{kl}E_mE_n - g_{ijklmno}\epsilon_{kl}\epsilon_{mn}E_o + X_{ijklmnop}\epsilon_{kl}\epsilon_{mn}\epsilon_{op}\end{aligned} \tag{2}$$

$$\begin{aligned}P_i = &b_{ij}E_j + Q_{ijkl}E_iE_jE_k + e_{ijk}\epsilon_{jk} + H_{ijklm}\epsilon_{jk}E_lE_m \\ &+ \beta_i\Theta - f_{ijklmn}\epsilon_{jk}\epsilon_{lm}E_n + g_{ijklmno}\epsilon_{jk}\epsilon_{lm}\epsilon_{no}\end{aligned} \tag{3}$$

$$\begin{aligned}&\dot{\Theta} = -\left[\sum_{i=1,3,5..}\left(\Gamma_i\frac{\partial\Psi}{\partial\Theta}\right)^i + \sum_{j=2,4,6..}\Gamma_j\left(\Gamma_j\frac{\partial\Psi}{\partial\Theta}\right)^{j-1}\left|\frac{\partial\Psi}{\partial\Theta}\right|\right] \\ &\text{where } \frac{\partial\Psi}{\partial\Theta} = \xi\Theta - \beta_iE_i - \Omega_{ij}\epsilon_{ij}\end{aligned} \tag{4}$$

where Γ_i are real constants. Equation (4) is the evolution equation for internal variable Θ. The detailed formulation can be found in [32]. In Eq. (2), P_iE_j term represents the antisymmetric stress tensor due to polarization–electric field interaction effects [7].

The equilibrium equation can be obtained from the conservation of linear momentum expression. Polarization-electric field interaction induces a nonlinear force term in the equilibrium equation. Equilibrium equation and Maxwell's equation can be written as

$$\sigma_{ji,j} + P_jE_{i,j} + f_i = \rho\ddot{u}_i \tag{5}$$

$$D_{i,i} = 0 \tag{6}$$

where $P_jE_{i,j}$ is the nonlinear body force term due to polarization–electric field interaction [7].

III. Weak Formulation

Considering a piezo ceramic of volume V with a boundary S, the electroelastic response of the material is given by the equation of motion and Maxwell's equation. The variational formulation is obtained by using principle of virtual work. In the absence of gravity force, the virtual work equation can be written by using Eqs. (5) and (6) multiplied by the corresponding virtual displacements and electric potential. The resulting expression is integrated over the volume of entire domain to get

$$\int_V (\sigma_{ji,j} + P_jE_{i,j} - \rho\ddot{u}_i)\delta u_i \,\mathrm{d}V + \int_V D_{i,i}\delta\phi \,\mathrm{d}V = 0 \tag{7}$$

where δu_i and $\delta\phi$ are the virtual displacement and virtual electric potential, respectively. Integrating Eq. (7) by parts one obtains

$$\int_V \frac{\partial(\sigma_{ji}\delta u_i)}{\partial x_j}\,\mathrm{d}V - \int_V \sigma_{ji}\frac{\partial\delta u_i}{\partial x_j}\,\mathrm{d}V + \int_V \frac{\partial(D_i\delta\phi)}{\partial x_i}\,\mathrm{d}V - \int_V D_i\frac{\partial\delta\phi}{\partial x_i}\,\mathrm{d}V + \underline{\int_V P_jE_{i,j}\delta u_i \,\mathrm{d}V} - \int_V \rho\ddot{u}_i\delta u_i \,\mathrm{d}V = 0 \tag{8}$$

In Eq. (8), the underlined term represents the virtual work due to the distributed nonlinear force caused by the polarization and electric field interaction. The total stress σ_{ji} can be divided into a linear symmetric (σ^L_{ji}) part, and a nonlinear part ($\sigma^{\mathrm{NL}}_{ji}$) due to the polarization–electric field interaction (P_jE_i) and the nonlinear terms in the constitutive relation due to quartic representation of strain and polarization in the free energy potential Ψ.

Separating the linear and nonlinear parts of the stress tensor, and by using Gauss divergence theorem, Eq. (8) can be written as

$$\int_V \rho\ddot{u}_i\delta u_i \,\mathrm{d}V + \int_V \sigma^L_{ji}\delta\varepsilon_{ij}\,\mathrm{d}V - \int_V D_i\delta E_i\,\mathrm{d}V - \int_V P_jE_{i,j}\delta u_i\,\mathrm{d}V + \int_V \sigma^{NL}_{ij}\delta\frac{\partial u_i}{\partial x_j}\,\mathrm{d}V = \int_s (\sigma_{ji}n_j\delta u_i + D_in_i\delta\phi)\,\mathrm{d}S \tag{9}$$

where $E_i = -\frac{\partial\phi}{\partial x_i}$; $\sigma_{ji}n_j = T_i$ is the applied boundary traction force; and $D_in_i = Q$ is the applied free charge on the boundary S. Substituting these terms in Eq. (9) leads to

$$\int_V \rho\ddot{u}_i\delta u_i \,\mathrm{d}V + \int_V \sigma^L_{ij}\delta\varepsilon_{ij}\,\mathrm{d}V - \int_V D_i\delta E_i\,\mathrm{d}V - \int_V P_jE_{i,j}\delta u_i\,\mathrm{d}V + \int_V \sigma^{NL}_{ij}\delta\frac{\partial u_i}{\partial x_j}\,\mathrm{d}V = \int_S T_i\delta u_i\,\mathrm{d}S + \int_S Q\delta\phi\,\mathrm{d}S \tag{10}$$

The term $\int_V \sigma^{NL}_{ij}\delta\frac{\partial u_i}{\partial x_j}\,\mathrm{d}V$ represents the work done by the nonlinear terms in the stress constitutive relations. On the boundary of piezoelectric domain, the surface is either free ($Q = 0$) or surface potential is specified (i.e. $\delta\phi = 0$). In both the cases $\int_S Q\delta\phi\,\mathrm{d}S$ term is zero.

IV. Finite Element Formulation

In this section, a layer-by-layer finite element formulation is developed for the smart composite plates subjected to static or dynamic loading. Coupled nonlinear electroelastic constitutive relations including the hysteresis effects, are used to derive the system equations. The mechanical tractions, or applied electric potential, or combination of both can be used as force on the plate.

A. Deformation Models

A layerwise theory is proposed for the analysis of smart plates [33]. The displacements, electric potential and internal variable (Θ) are represented as a product of in-plane and out-of-plane approximating functions. The axis system of the problem is taken as Cartesian coordinate system as shown in Fig. 1. The displacement fields, electric potential and internal variable (u, v, w, ϕ, Θ) in each element are represented as

$$\begin{aligned}
u(x,y,z,t) &= \sum_{i=1}^{n_u}\sum_{j=1}^{n_z} u_{ij}(t)N_i(x,y)\bar{M}_j(z)\\
v(x,y,z,t) &= \sum_{i=1}^{n_u}\sum_{j=1}^{n_z} v_{ij}(t)N_i(x,y)\bar{M}_j(z)\\
w(x,y,z,t) &= \sum_{i=1}^{n_u}\sum_{j=1}^{n_w} w_{ij}(t)N_i(x,y)\bar{M}_j(z)\\
\phi(x,y,z,t) &= \sum_{i=1}^{n_u}\sum_{j=1}^{n_w} \phi_{ij}(t)N_i(x,y)\bar{M}_j(z)\\
\Theta(x,y,z,t) &= \sum_{i=1}^{n_u}\sum_{j=1}^{n_w} \Theta_{ij}(t)N_i(x,y)\bar{M}_j(z)
\end{aligned} \tag{11}$$

where u, v and w are the displacements along x, y and z axis respectively; ϕ is electric potential; and Θ is the internal variable. Further, $N_i(x,y)$ are the in-plane basis functions; $\bar{M}_j$ are the out-of-plane basis functions; u_{ij}, v_{ij} and w_{ij} are the nodal displacements; ϕ_{ij} and Θ_{ij} are electric potential and internal variable at the nodes. Also, n_u is the number of in-plane basis functions used for u, v, w, ϕ and Θ, respectively; n_z is the number of out-of-plane basis functions used for u and v approximations; and n_w is the number of basis functions used for w, ϕ and Θ approximations. Legendre polynomials based hierarchic basis functions are used. These functions have primary nodes in the corners of the triangles and all other internal nodes are fictitious. In this study, specifically, piecewise (C^0 functions) cubic approximation has been taken for all the displacements, electric potential and internal variable in the in-plane and out-of-plane directions. For the given approximation, i.e., cubic, there are 10 nodes in the in-plane and 4 nodes in the transverse direction.

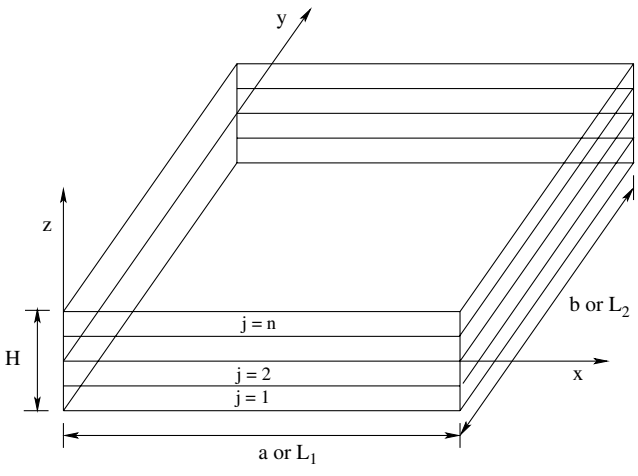

Fig. 1 Axis system of the plate.

The core material of the plate can be isotropic or a composite laminate. The core is electrically inactive; hence the core can be completely characterized by the displacement field with components u, v and w. Thus, for the core, 3 degrees of freedom are specified at each node, corresponding to the in-plane displacement components (u, v) and the transverse displacement w. In the piezo layers, the local potential field ϕ has to be determined along with the three displacement components (u, v w). In the case of dynamic analysis the internal variable Θ is also taken as a field variable in the piezo electric material. Hence, for the piezo layers 5 degrees of freedom (u, v w, ϕ, Θ) have to be considered at each node.

B. Equilibrium Equations in Matrix Form

Substituting the displacement field [Eq. (11)] and constitutive relations [Eqs. (2) and (3)] in Eq. (10), the set of nonlinear dynamic equations can be written in matrix form as

$$[M]\{\ddot{q}\} + [K]^L\{q\} + [K_1(\{q\})]\{q\} + [K_2(\{q\})]\{q\} + [K_3(\{q\})]\{q\} = \{F(t)\} \tag{12}$$

where $\{F(t)\}$ is the force vector due to traction; displacement vector $\{q\} = \{u, v, w, \phi, \Theta\}^T$; $[M]$ is the mass matrix; $[K]^L$ is the linear stiffness matrix. Note that in the dynamic formulation, the internal variable Θ is an additional unknown, with its instantaneous value governed by the evolution equation [Eq. (4)]. The dynamic equations contain four nonlinear terms: 1) $[K_1]$, the stiffness matrix due to nonlinear force term ($P_i E_{j,i}$) in the equilibrium equations, 2) $[K_2]$, the stiffness due to antisymmetric stress tensor ($P_i E_j$), 3) $[K_3]$, the stiffness matrix corresponding to the nonlinear terms arising out of the quartic terms associated with strain and electric field in free energy Ψ [Eq. (1)], and 4) the nonlinearity associated with the evolution of internal variable [Eq. (4)].

While performing the dynamic analysis, the stiffness terms in Eq. (12) are linearized by substituting the displacement vector $\{q\}$ from the previous time instant. The updated stiffness matrix at every time instant can be written as

$$[K]_t = [K]^L + [K_1(q_{t-1})] + [K_2(q_{t-1})] + [K_3(q_{t-1})] \tag{13}$$

Using Eq. (13), the response of the plate [Eq. (12)] can be written as

$$\begin{bmatrix} M_{11} & 0 & 0 & 0 & 0 \\ 0 & M_{22} & 0 & 0 & 0 \\ 0 & 0 & M_{33} & 0 & 0 \\ 0 & 0 & 0 & 0 & 0 \\ 0 & 0 & 0 & 0 & 0 \end{bmatrix} \begin{Bmatrix} \{\ddot{u}\} \\ \{\ddot{v}\} \\ \{\ddot{w}\} \\ \{\ddot{\phi}\} \\ \{\ddot{\Theta}\} \end{Bmatrix} + \begin{bmatrix} K_{uu} & K_{uv} & K_{uw} & K_{u\phi} & K_{u\Theta} \\ K_{vu} & K_{vv} & K_{vw} & K_{v\phi} & K_{v\Theta} \\ K_{wu} & K_{wv} & K_{ww} & K_{w\phi} & K_{w\Theta} \\ K_{\phi u} & K_{\phi v} & K_{\phi w} & K_{\phi\phi} & K_{\phi\Theta} \\ 0 & 0 & 0 & 0 & 0 \end{bmatrix} \begin{Bmatrix} \{u\} \\ \{v\} \\ \{w\} \\ \{\phi\} \\ \{\Theta\} \end{Bmatrix} = \begin{Bmatrix} f_u(t) \\ f_v(t) \\ f_w(t) \\ 0 \\ 0 \end{Bmatrix} \tag{14}$$

where $K_{u\Theta}$, $K_{v\Theta}$ and $K_{w\Theta}$ are the updated stiffness terms corresponding to internal variable and mechanical coupling; $K_{\phi\Theta}$ represents the coupling between internal variable and electric field. These terms can be obtained as

$$[K_{u\Theta}] = \int_V -\Omega_{11}\Theta\frac{\partial\delta u}{\partial x}\,\mathrm{d}V \tag{15}$$

$$[K_{v\Theta}] = \int_V -\Omega_{22}\Theta\frac{\partial\delta v}{\partial y}\,\mathrm{d}V \tag{16}$$

$$[K_{w\Theta}] = \int_V -\Omega_{33}\Theta\frac{\partial\delta w}{\partial z}\,\mathrm{d}V \tag{17}$$

$$[K_{\phi\Theta}] = \int_V \beta_3\Theta\left(-\frac{\partial\delta\phi}{\partial z}\right)\mathrm{d}V \tag{18}$$

Here, it can be noted that linear stiffness matrix $[K]^L$ is used to obtain the modal system of the plate. Equation (14) can be written in simplified form as

$$\begin{bmatrix} M_{UU} & 0 & 0 \\ 0 & 0 & 0 \\ 0 & 0 & 0 \end{bmatrix} \begin{Bmatrix} \{\ddot{U}\} \\ \{\ddot{\phi}\} \\ \{\ddot{\Theta}\} \end{Bmatrix} + \begin{bmatrix} K_{UU} & K_{U\phi} & K_{U\Theta} \\ K_{\phi U} & K_{\phi\phi} & K_{\phi\Theta} \\ 0 & 0 & 0 \end{bmatrix} \begin{Bmatrix} \{U\} \\ \{\phi\} \\ \{\Theta\} \end{Bmatrix} = \begin{Bmatrix} F \\ 0 \\ 0 \end{Bmatrix} \tag{19}$$

where, U is the mechanical displacement field ($\{U\} = \{u, v, w\}^T$); $[K_{UU}]$ is the stiffness due to mechanical part; $[K_{U\phi}]$ is the stiffness due to electromechanical coupling; $[K_{\phi\phi}]$ is the stiffness due to electric part; $[K_{U\Theta}]$ is stiffness due to mechanical and internal variable coupling part and $[K_{\phi\Theta}]$ is stiffness due to electric and internal variable coupling. Depending on the past strain, electric field and the internal variable history, the rate of internal variable $\dot{\Theta}$ at the present time can be calculated based on the evolution equation [Eq. (4)]. Hence, Θ is a known quantity at that instant. Therefore, Eq. (19) can be modified as

$$\begin{bmatrix} M_{UU} & 0 \\ 0 & 0 \end{bmatrix} \begin{Bmatrix} \{\ddot{U}\} \\ \{\ddot{\phi}\} \end{Bmatrix} + \begin{bmatrix} K_{UU} & K_{U\phi} \\ K_{\phi U} & K_{\phi\phi} \end{bmatrix} \begin{Bmatrix} \{U\} \\ \{\phi\} \end{Bmatrix} = \begin{Bmatrix} \{F\} - [K_{U\Theta}]\{\Theta\} \\ -[K_{\phi\Theta}]\{\Theta\} \end{Bmatrix} \tag{20}$$

If actuation potential $\{\phi^A\}$ is specified on the surface of the piezo layer the Eq. (20) can be rewritten as

$$\begin{bmatrix} M_{UU} & 0 \\ 0 & 0 \end{bmatrix} \begin{Bmatrix} \{\ddot{U}\} \\ \{\ddot{\phi}\} \end{Bmatrix} + \begin{bmatrix} K_{UU} & K^S_{U\phi} \\ K^S_{\phi U} & K^S_{\phi\phi} \end{bmatrix} \begin{Bmatrix} \{U\} \\ \{\phi\}^S \end{Bmatrix} = \begin{Bmatrix} F(t) - [K_{U\Theta}]\{\Theta\} - [K^A_{U\phi}]\{\phi^A\} \\ -[K_{\phi\Theta}]\{\Theta\} - [K^A_{\phi\phi}]\{\phi^A\} \end{Bmatrix} \tag{21}$$

where $\{\phi\}^S$ is the induced potential; $[K_{U\phi}]^S$ and $[K_{\phi\phi}]^S$ are the stiffness associated with induced potential $\{\phi\}^S$. As there is no inertial term associated with the electric field, Eq. (21) can be decoupled into an algebraic equation and a differential equation, which can be written as

$$[M]\{\ddot{U}\} + [K_{UU}]\{U\} + [K^S_{U\phi}]\{\phi^S\} = \{F(t)\} - [K_{U\Theta}]\{\Theta\} - [K^A_{U\phi}]\{\phi^A\} \tag{22}$$

$$[K^S_{\phi U}]\{U\} + [K^S_{\phi\phi}]\{\phi^S\} = -[K_{\phi\Theta}]\{\Theta\} - [K^A_{\phi\phi}]\{\phi^A\} \tag{23}$$

The induced electric potential, from Eq. (23), can be written as

$$\{\phi^S\} = -[K^S_{\phi\phi}]^{-1}([K^S_{\phi U}]\{U\} + [K_{\phi\Theta}]\{\Theta\} + [K^A_{\phi\phi}]\{\phi^A\}) \tag{24}$$

Substituting Eq. (24) in Eq. (22), equation of motion can be written as

$$[M]\{\ddot{U}\} + ([K_{UU}] - [K^S_{U\phi}][K^S_{\phi\phi}]^{-1}[K^S_{\phi U}])\{U\} = \{F(t)\} + ([K^S_{U\phi}][K^S_{\phi\phi}]^{-1}[K_{\phi\Theta}] - [K_{U\Theta}])\{\Theta\} + ([K^S_{U\phi}][K^S_{\phi\phi}]^{-1}[K^A_{\phi\phi}] - [K^A_{U\phi}])\{\phi^A\} \tag{25}$$

C. Modal Response of Smart Plates

In the modal analysis, the displacement field $\{U\}$ can be represented as linear combination of modal matrix $[\Phi]$ and modal degrees of freedom $\{\eta(t)\}$, as

$$\{U\} = [\Phi]\{\eta(t)\} \tag{26}$$

where $[\Phi]$ is the modal matrix obtained using the linear dynamic equation.

Substituting the expression for displacement given in Eq. (26) in Eq. (25) and premultiplying with $[\Phi]^T$, equation of motion can be rewritten as

$$[\tilde{M}]\{\ddot{\eta}\} + [\tilde{K}]\{\eta\} = \{\tilde{F}\} \tag{27}$$

where, $[\tilde{M}]$, $[\tilde{K}]$ and $\{\tilde{F}\}$ are the modal mass matrix, modal stiffness matrix and modal force, respectively. Modal matrices can be obtained as

$$[\tilde{M}] = [\Phi]^T[M][\Phi] \tag{28}$$

$$[\tilde{K}] = [\Phi]^T([K_{UU}] - [K^S_{U\phi}][K^S_{\phi\phi}]^{-1}[K^S_{\phi U}])[\Phi] \tag{29}$$

$$\{\tilde{F}\} = [\Phi]^T\{\{F(t)\} + ([K^S_{U\phi}][K^S_{\phi\phi}]^{-1} - [K_{\phi\Theta}] - [K_{U\Theta}])\{\Theta\} + ([K^S_{U\phi}][K^S_{\phi\phi}]^{-1}[K^A_{\phi\phi}])\{\phi^A\}\} \tag{30}$$

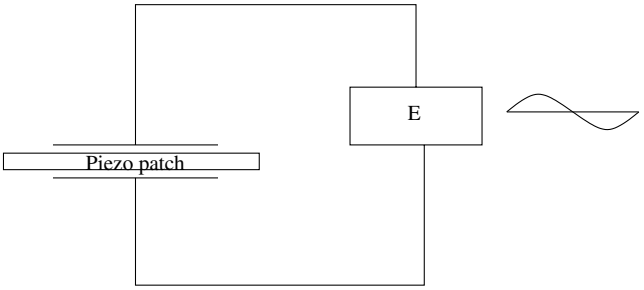

Fig. 2 Piezo patch under varying electric field.

$$\sigma^{\mathrm{LH}}_{ij} = C_{3333}\epsilon_{33} - e_{333}E_k - \Omega_{33}\Theta \tag{33}$$

$$P^{\mathrm{LH}}_i = b_{33}E_3 + e_{333}\epsilon_{33} + \beta_3\Theta \tag{34}$$

$$\dot{\Theta} = -\left[\sum_{i=1,3,5..}\left(\Gamma_i\frac{\partial\Psi}{\partial\Theta}\right)^i + \sum_{j=2,4,6..}\Gamma_j\left(\Gamma_j\frac{\partial\Psi}{\partial\Theta}\right)^{j-1}\left|\frac{\partial\Psi}{\partial\Theta}\right|\right] \quad \text{where } \frac{\partial\Psi}{\partial\Theta} = \xi\Theta - \beta_3E_3 - \Omega_{ij}\epsilon_{33} \tag{35}$$

The nonlinear electroelastic constitutive relations (applicable for this one-dimensional problem) can be written as

$$\sigma_{33} = C_{3333}\epsilon_{33} - e_{333}E_3 - \Omega_{33}\Theta - P_3E_3 \underline{- H_{33333}E_3E_3E_3 + f_{333333}\epsilon_{33}E_3E_3 - g_{3333333}\epsilon_{33}\epsilon_{33}E_3 + X_{33333333}\epsilon_{33}\epsilon_{33}\epsilon_{33}} \tag{36}$$

$$P_3 = b_{33}E_3 + e_{333}\epsilon_{33} + \beta_3\Theta + \underline{Q_{3333}E_3E_3E_3 + H_{33333}\epsilon_{33}E_3E_3 - f_{333333}\epsilon_{33}\epsilon_{33}E_3 + g_{3333333}\epsilon_{33}\epsilon_{33}\epsilon_{33}} \tag{37}$$

D. Nonlinear Static Equations

For the nonlinear static problem, the equilibrium equations are obtained by neglecting the inertia term and the internal variable Θ in Eq. (12). It can be written as

$$[K]^L\{x\} + [K_1(\{x\})]\{x\} + [K_2(\{x\})]\{x\} + [K_3(\{x\})]\{x\} = \{F\} \tag{31}$$

where $\{x\} = \{u, v, w, \phi\}^T$. For the static linear case, the equilibrium equation can be written as

$$[K]\{x\} = \begin{bmatrix} K_{UU} & K_{U\phi} \\ K_{\phi U} & K_{\phi\phi} \end{bmatrix}\begin{Bmatrix} \{U\} \\ \{\phi\} \end{Bmatrix} = \begin{Bmatrix} F \\ 0 \end{Bmatrix} \tag{32}$$

where $\{U\}$ is the mechanical displacement vector ($\{u, v, w\}^T$); $[K_{UU}]$ is the stiffness due to mechanical part; $[K_{U\phi}]$ is the stiffness due to electromechanical coupling; $[K_{\phi\phi}]$ is the stiffness due to electric part.

V. Results and Discussion

A. Variation of Strain and Polarization with Electric Field

To evaluate the effect of nonlinearity in the constitutive relations, hysteresis loops have been generated using two different sets of constitutive relations, namely, (i) linear constitutive relations with nonlinear equation for internal variable and (ii) nonlinear constitutive relations with nonlinear equation for internal variable [Eqs. (2–4)]. Considering a piezo patch subjected to an external time varying electric field of amplitude 2 kV/mm along z-direction as shown in Fig. 2, the linear electroelastic constitutive relations with hysteresis effects applicable for this one-dimensional problem can be written as

$$\dot{\Theta} = -\left[\sum_{i=1,3,5..}\left(\Gamma_i\frac{\partial\Psi}{\partial\Theta}\right)^i + \sum_{j=2,4,6..}\Gamma_j\left(\Gamma_j\frac{\partial\Psi}{\partial\Theta}\right)^{j-1}\left|\frac{\partial\Psi}{\partial\Theta}\right|\right] \quad \text{where } \frac{\partial\Psi}{\partial\Theta} = \xi\Theta - \beta_3E_3 - \Omega_{33}\epsilon_{33} \tag{38}$$

The material considered for the study is PZT-5H and values of all material constants used for generating the hysteresis loops are listed in the Tables 1–3 [15]. The frequency of electric field is taken as 0.0165 Hz. The resulting hysteresis loops along with the experimental data [34] is shown in Fig. 3. From the figure it can be seen that the effect of additional nonlinear terms [the underlined terms in the constitutive relations in Eqs. (36) and (37)] is more predominant near the saturation polarization zone. Further, the area of the hysteresis loop is not much affected by these nonlinear terms in the constitutive relations.

It is shown in the following that the relation between strain and electric field is in the form of butterfly loop, when the electric field is oscillated above the coercive electric field (corresponding to saturation polarization, referred to as $E_{C\max}$, which in this case is 1 kV/mm, from Fig. 3), whereas it need not be in the form of butterfly loop when the amplitude of electric field is below coercive electric field.

Table 1 Material properties of PZT

C_{33}	e_{3333}	b_{33}
GPa	$\mathrm{C\,m^{-2}}$	$\mathrm{C^2\,N^{-1}\,m^{-2}}$
117	23.3	1.30095E − 8

Table 2 Constants in internal variable equation

ξ GPa	Ω_{33} GPa	β_3 C m^{-2}	H_{33333}	Q_{3333}	f_{333333}	$g_{3333333}$	$X_{33333333}$
0.00106	0.323	0.2594	−5.2E − 12	−7E − 20	0	0	0

Table 3 Values of Γ, m N^{-1} S^{-1}

Γ_1	Γ_2	Γ_3	Γ_4	Γ_5	Γ_6	Γ_7
2.26E − 11	3.16E − 10	13.2E − 8	11.0E − 8	2.72E − 7	4.47E − 07	3.6106E − 06

Using the constitutive relations [Eqs. (36–38)] variation of polarization versus electric field and variation of strain versus electric field are analyzed for unsymmetric variation of electric field. For this study, the analysis is carried out for a free piezo patch subjected to an external time varying electric field along z-direction, the variation of applied electric field, is shown in Fig. 4. The electric field is oscillated initially for two full cycles ranging from 2 to −2 kV/mm, then to 0.3 to −1.25 kV/mm; and then to 0.5 to −1.25 kV/mm and finally to 1.25 to −1.25 kV/mm. Frequency of electric field is taken as 0.0165 Hz. The material considered for the study is PZT-5H and the material properties are given in Tables 1–3.

The polarization–electric field and strain-electric field variations are shown in Figs. 5 and 6, respectively. The points in the time signal of the electric field are marked with the alphabets a to z (Fig. 4), and the corresponding points are indicated in Figs. 5 and 6.

For the purpose of clarity, the variation of strain, shown in Fig. 6, is split into three subplots as shown in Fig. 7. The variation of strain during the time period a to l (in Fig. 4) shows a butterfly loop, as shown in the subplot (Fig. 7a). For the time interval l to p in Fig. 4, the electric field is varied unsymmetrically. In this interval, the strain variation shows a single loop (Fig. 7b) which increases with increase in amplitude of the electric field from point p to 0.3 kV/mm (point m); then from −1.25 kV/mm (point n) to 0.5 kV/mm (point o) and back to −1.25 kV/mm (point p). For the time interval p to z, the field is varied from −1.25 to 1.25 kV/mm. The corresponding variation in strain (Fig. 7c) shows a butterfly loop.

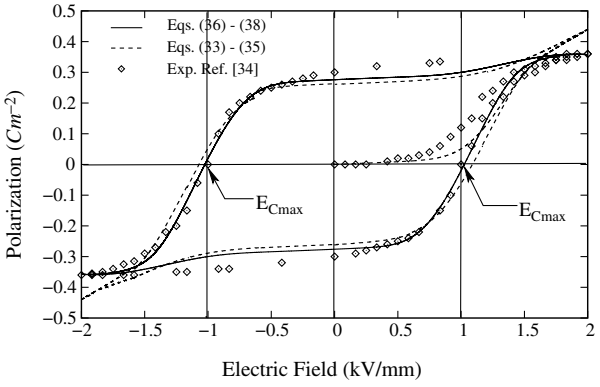

Fig. 3 Variation of polarization with electric field (hysteresis loop).

This result clearly indicates that when the amplitude of the electric field is less than the coercive electric field (corresponding to saturation polarization, which in this case is 1 kV/mm) the strain variation does not exhibit butterfly type loop. However, if the amplitude is greater than $E_{C\max}$, strain variation exhibits a butterfly loop.

B. Static and Dynamic Analysis of Smart Composite Plates

Using the finite element formulation derived in the previous section, static and dynamic analyses of smart plate is carried out with single and multiple (segmented) piezo patches. The validation of the formulation and the finite element code has been carried out by comparing the theoretical results with the experimental results given by Crawley and Lazarus [16]. Further, nonlinear analysis has been carried out to study the effect of polarization–electric interaction in the static analysis. Finally, dynamic analysis has been carried out to study the influence of dissipation due to the polarization–electric field hysteresis effect on the response of a composite plate with surface mounted piezo layers in actuation.

C. Linear and Nonlinear Static Analysis of Composite Plate with Segmented Piezo Patches

Consider a smart composite plate with the edge fixed along $x = 0$ (cantilevered), as shown in Fig. 8. The composite plate consists of 15

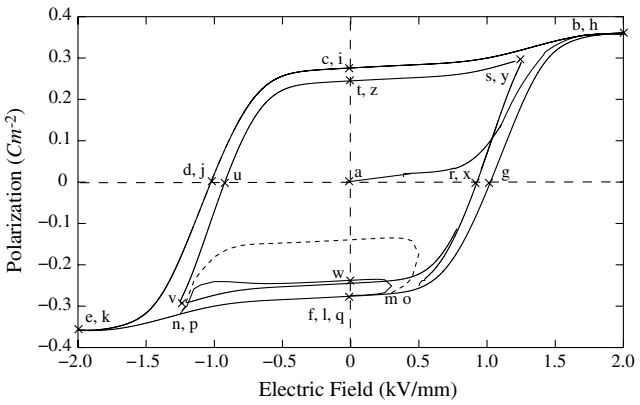

Fig. 5 Variation of polarization with unsymmetric oscillation of electric field.

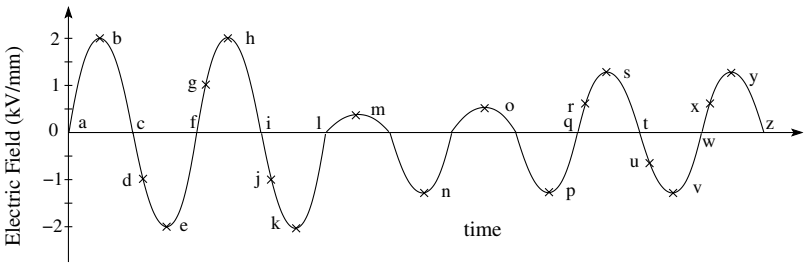

Fig. 4 Variation of electric field.

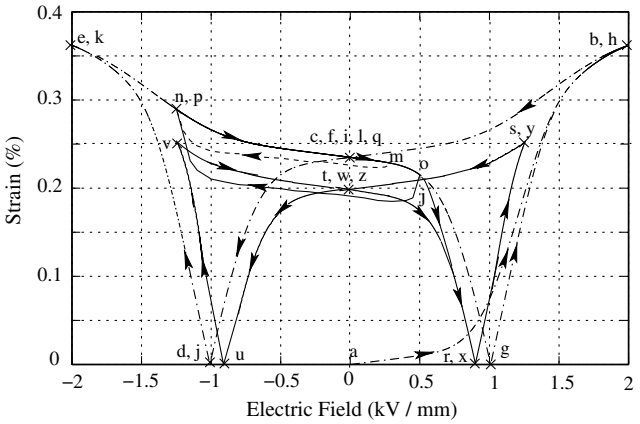

Fig. 6 Variation of strain with unsymmetric oscillation of electric field.

piezo patches on either side. The length of the plate L_1 is 292 mm and width of the plate L_2 is 152 mm. The core material consists of graphite-epoxy and has 0.83 mm thickness. The ply orientation of the core is $[0/\pm 45^0]_s$. Piezo patches are made of PZT-G1195 and have a thickness of 0.25 mm. Properties of piezo and composite materials used in the analysis are given in Table 4. The interface between the core and the piezo patch is grounded; and the other surface is subjected to an applied electric potential. A constant electric field of 394 V/mm with opposite polarity is applied on either side of the plate. Linear analysis is carried out initially by neglecting the nonlinear stiffness matrices $[K_1]$, $[K_2]$ and $[K_3]$ [Eq. (31)]. The longitudinal bending, transverse bending and twist deflections are nondimensionalized as

$$\begin{aligned}&\text{Longitudinal bending} = w_2/L_2\\ &\text{Transverse bending} = \frac{1}{L_2}\left[w_2 - \frac{(w_3 + w_1)}{2}\right]\\ &\text{Twisting} = [w_3 - w_1]/L_2\end{aligned} \tag{39}$$

where L_2 is width of the plate; w_2 is transverse deflection along the centerline of the plate in longitudinal direction; w_1 and w_3 are the transverse deflections along the edges A and B (Fig. 8), respectively.

The results of the linear and nonlinear analysis, along with the experimental data of Crawley and Lazarus [16], are shown in Fig. 9. The number of unknowns for the present finite element analysis is 152,410. Finite element results of Ha et al. [25] are also given in the figure with a dashed line. Direct (Picard) iteration method is used to obtain the nonlinear solution. Figure 9a shows the longitudinal bending along the length of the plate. From the figure it can be seen that the results present linear correlate well with the experimental data. Further, the results of present linear analysis and numerical results of Ha et al. [25] give the same longitudinal bending. For nonlinear case, the longitudinal bending values are higher than the linear values, with the nonlinearity showing a softening trend.

Figure 9b shows transverse bending. The results of the present linear analysis and the numerical results of Ha et al. [25] show a similar trend. Transverse bending deflection for nonlinear case is slightly lower than that obtained with linear analysis. In this case, the nonlinear effect shows hardening effect. Figure 9c represents the twist of the plate. From the figure it can be seen that the linear twist of present analysis correlates better with the experimental data, as compared with the finite element results of Ha et al. [25]. Nonlinear effect in this case shows softening effect and the nonlinear effect induces more twist deflection.

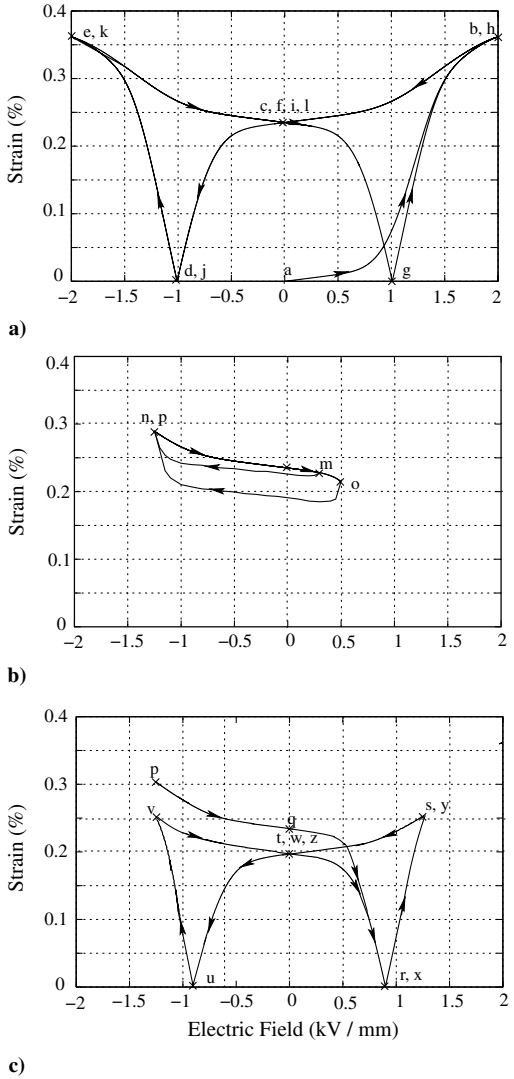

Fig. 7 Detailed representation of variation of strain with unsymmetric oscillation of electric field: a) corresponds to electric actuation path *a* to *l*, b) corresponds to path *l* to *p*, and c) corresponds to path *p* to *z* in Fig. 4.

D. Dynamic Analysis

Dynamic analysis of smart plates is carried out by using the nonlinear finite element formulation including the dissipation due to hysteresis effects. Response of the plate is obtained by using modal analysis. Initially validation of the formulation is carried out by obtaining the natural frequencies of a square composite plate with linear constitutive relations and equilibrium equation; and comparing with the analytical results given by Heyliger and Saravanos [28]. The response of the plate is obtained for three different cases to study the effects of polarization–electric field hysteresis and nonlinear stiffness terms: 1) with linear stiffness matrix $[K]^L$ and no hysteresis effects, 2) with linear stiffness matrix $[K]^L$ and hysteresis effects, and 3) including all nonlinear terms and hysteresis effects.

A simply-supported square plate with a three-layered composite core is considered for the analysis. The ply-orientation of the core is [0/90/0] and a piezo layer is mounted on the top and bottom faces. Thicknesses of composite laminae and piezo layers are taken as 0.27 H and 0.1 H, where H is the thickness of the plate. The materials used are graphite-epoxy and PZT-4, for which the properties are given in Table 5. Simply-supported boundary conditions have been employed as

$$\begin{aligned}&u(x,0,z) = u(x,b,z) = v(0,y,z) = v(a,y,z) = 0\\ &w(x,0,z) = w(x,b,z) = w(0,y,z) = w(a,y,z) = 0\end{aligned} \tag{40}$$

All four vertical edges of the piezo layers are grounded. Natural frequencies are obtained for two kinds of electric boundary conditions for the piezo layer, namely, OC and CC. For OC boundary condition, the top and bottom faces of the piezo remain free (zero electric displacement) and for CC boundary condition the top and

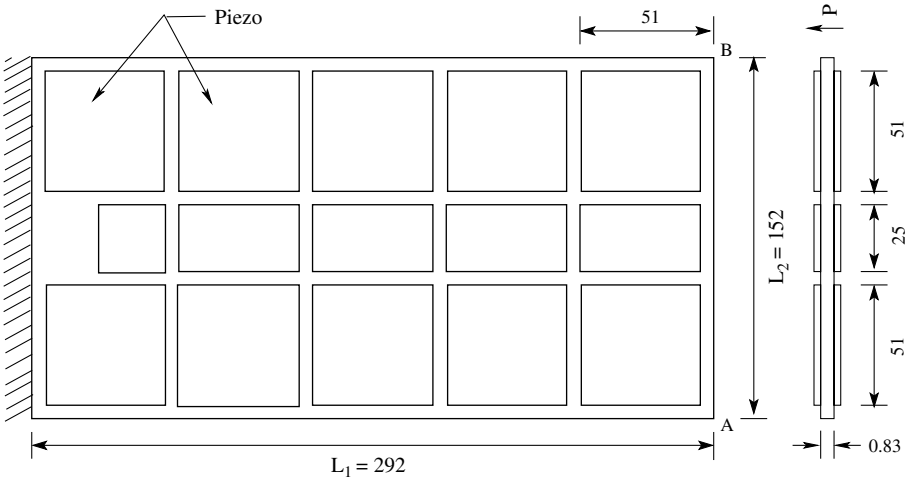

Fig. 8 Schematic representation of $[0/\pm 45^0]_s$ cantilever plate with segmented piezo patches (dimensions are in mm).

bottom faces are shorted and grounded, i.e., electric potential has been specified as zero.

Two different length-to-thickness ratios ($S = 4$ and 50) are considered for the analysis. For validating the results, the densities of the piezo and composite ply are taken as unity. The number of degrees of freedom considered in the analysis is 10200. The predicted natural frequency parameters corresponding to six thickness modes for OC and CC electric boundary conditions along with the analytical results by Heyliger and Saravanos [28] are given in Table 6. The natural frequency parameter γ is obtained as $\omega/100$, where ω is the natural frequency in radians per second. The finite element results by Saravanos et al. [26] (with a mesh density 12×12) are also presented in the Table 6 for comparison. It may be noted that in [26], only the results corresponding to fundamental mode are given.

From the results, it can be seen that the natural frequency parameter obtained by the present study, for the OC boundary condition, is slightly more than the analytical results for similar boundary conditions given in [28]. Further, the OC electric boundary condition shows stiffened behavior when compared with CC electric boundary condition.

E. Response of the Plate

The free vibration response of the smart plate, subjected to an impulse electric or mechanical loading, is obtained by mode superposition method. Newmark-β scheme is used for the time integration. First a verification of the modal convergence is carried out to study the effect of modal dependency on the transverse deflection.

For the analysis, a three ply laminated composite plate with continuous piezo layers on either side of the plate as shown in Fig. 10 is considered. The ply orientation of the plate core is [0/90/0] and thickness of each lamina is 2.67 mm. In-plane dimension of the plate is 500 × 500 mm. Each piezo layer is 1 mm thick. The composite layers are made of graphite-epoxy, and PZT-4 is used for the piezo layers. The material properties of the PZT-4 and graphite-epoxy are listed in Table 5.

Table 4 Material properties of graphite-epoxy and piezoceramic

Property	Graphite-epoxy	PZT-G1195
E_{ll}, GPa	147.00	63.0
E_{tt}, GPa	9.7	63.0
G_{lt}, GPa	6.0	24.2
G_{tt}, GPa	6.0	24.2
ν_{lt}, GPa	0.3	0.3
ν_{tt}, GPa	0.3	0.3
d_{31}, pm/V	0.0	310.0
d_{32}, pm/V	0.0	310.0
d_{33}, pm/V	0.0	374.0
d_{24}, pm/V	0.0	584.0
ε_{11}, 10^{-10} F/m	153.00	153.0
ε_{22}, 10^{-10} F/m	153.00	153.0
ε_{33}, 10^{-10} F/m	153.00	150.0

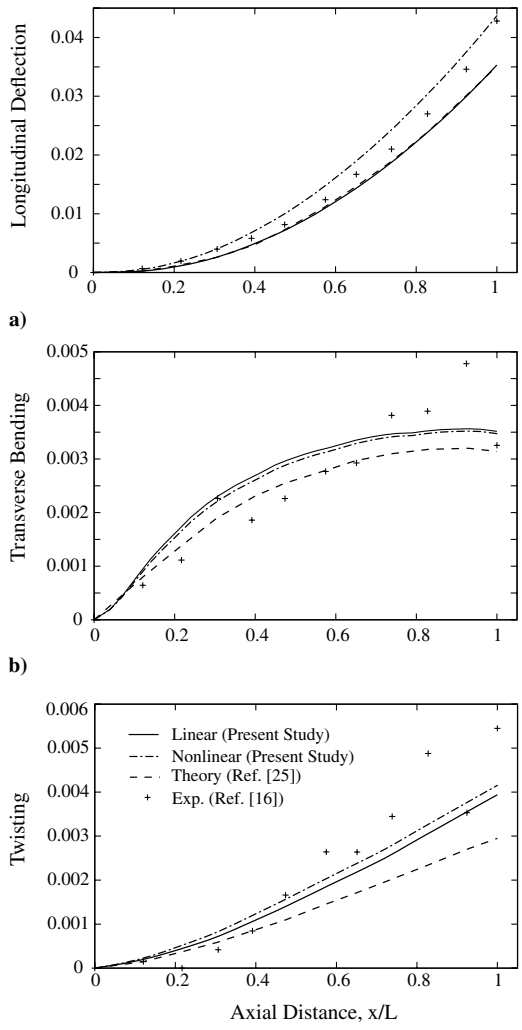

Fig. 9 Deformations of $[0/\pm 45]_s$ cantilever plate.

Table 5 Material properties of PZT-4 (poling along z-axis) and graphite-epoxy (from [28])

Properties	Units	PZT-4	Graphite-epoxy
E_1	GPa	81.3	132.38
E_2	GPa	81.3	10.756
E_3	GPa	64.5	10.756
ν_{12}	——	0.329	0.24
ν_{13}	——	0.432	0.24
ν_{23}	——	0.432	0.49
G_{44}	GPa	25.6	3.606
G_{55}	GPa	25.6	5.654
G_{66}	GPa	30.6	5.654
e_{31}	C m^{-2}	−5.20	0
e_{32}	C m^{-2}	−5.20	0
e_{33}	C m^{-2}	15.08	0
$\varepsilon_{11}/\varepsilon_0$	——	1475	3.5
$\varepsilon_{22}/\varepsilon_0$	——	1475	3.0
$\varepsilon_{33}/\varepsilon_0$	——	1300	3.0

Table 6 Frequency parameters for [PZT/0/90/0/PZT] composite plate with surface mounted piezo layers

Present study		Values from [28]		Values from [26]	
CC	OC	CC	OC	CC	OC
		$a/h = 4$			
55,588	57,104	57,074	57,089	57,177	59,475
189,986	191,336	191,301	191,304	——	——
254,989	250,789	250,769	250,770	——	——
274,061	274,961	274,941	274,941	——	——
362,014	362,501	362,492	362,552	——	——
390,996	391,038	391,036	381,049	——	——
		$a/h = 50$			
585.12	618.82	618.11	618.12	595.74	651.07
15,561.7	15,681.9	15,681.6	15,681		
21,405.9	21,494.1	21,492.8	21,493		
209,695	209,710	209,704	209,707		
210,519	210,525	210,522	210,573		
378,098	378,106	378,104	378,105		

1. Modal Convergence

To verify the modal convergence, it is assumed that the top and bottom surfaces of the piezo are grounded (CC condition) along with all four vertical edges. Simply-supported boundary conditions as given in Eq. (40) are employed. For obtaining the natural frequencies, the nonlinear stiffness matrices $[K_1]$, $[K_2]$, $[K_3]$ and hysteresis effects are not considered. The first six natural frequencies of the plate are listed in Table 7 and the corresponding mode shapes are shown in Fig. 11. From Fig. 11, it can be observed that all the 6 modes are bending modes. The natural frequency in third (and fifth) bending modes are more than that of the second (and fourth) bending modes, respectively, even though the mode shapes look similar. The reason for this behavior is because of the ply-orientation.

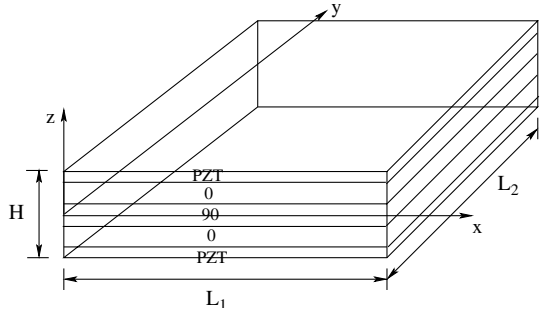

Fig. 10 Schematic representation of a [PZT/0/90/0/PZT] plate.

Table 7 Natural frequencies of smart plate for CC condition

Sl No.	Frequency, rad/s	Type
1	1105.39	Bending-1
2	2499.64	Bending-2
3	3163.80	Bending-2
4	4354.21	Bending-3
5	4925.43	Bending-3
6	6560.10	Bending-4

The response of the plate is obtained for an impulse load due to actuation voltage, which is given as

$$\phi(x, y, \pm H/2) = \phi_0 \quad 0 \le t \le 0.001 \text{ s}$$
$$= 0 \qquad t > 0.001 \text{ s} \tag{41}$$

Verification of the modal convergence is carried out initially to study the effect of modal dependency on the transverse deflection. Transverse deflection corresponding to the first mode, first three modes and first six modes are obtained, when the plate is subjected to an electric potential of $\phi_0 = 400$ V for 0.001 s (impulse load). In obtaining the response of the plate, stiffness due to higher order terms ($[K_3]$) and nonlinear stiffness due to polarization–electric field interaction ($[K_1]$ and $[K_2]$) are not included. Time step considered for the integration is 0.0001 s. The response at the material point $(0.5L_1/0.5L_2/0)$ is shown in Fig. 12. It can be seen from the figure that the influence of higher modes is negligible on the transverse deflection of the plate.

Therefore, in the nonlinear dynamic analysis, only the fundamental mode is considered.

2. Response with Linear Stiffness $[K]^L$ and with and Without Hysteresis Effects

To study the effect of dissipation due to polarization–electric field hysteresis, response of the plate is obtained for an applied impulsive electric field. The plate is simply supported on all four edges as given in Eq. (40). The interface between the core and the piezo layer, and all four vertical edges of the piezo layer are grounded. An electric potential ϕ_0 of 400 V is applied on the top and bottom faces of the plate as given in Eq. (41) for 0.001 s (impulse). Time step for the integration is considered as 0.0001 s. The dynamic response of the plate is obtained for two cases, namely, with and without hysteresis effect. The response at the point $(0.5L_1/0.5L_2/0)$ is shown in Fig. 13, for both cases. From the figure it can be seen that the dynamic response without hysteresis effect shows a sinusoidal behavior with an amplitude of 0.11 mm and a frequency equal to 1105 rad/s (which is the fundamental natural frequency of the plate, as given in Table 7). However the dynamic response with hysteresis effect shows decaying amplitude. The decay in amplitude is observed to be linear which is similar to friction-type damping. In addition, the frequency of oscillation is found to be 1060 rad/s. It can be seen that initially the response of the plate with hysteresis effect is slightly more than that of the response without hysteresis effect. The reason for this behavior could be attributed to the inclusion of the additional variable Θ in the problem.

This numerical example highlights the importance of modeling the hysteresis effects while analyzing the response of smart structures. Further more, it is found that the dissipation effect is significant and it can lead to temperature rise in the piezo material.

3. Response of the Plate with all Nonlinear Stiffness and Hysteresis Effects

The dynamic response of the plate with and without nonlinear stiffness terms ($[K_1]$, $[K_2]$ and $[K_3]$) and including hysteresis effect is evaluated for an impulse actuation of 400 V/mm acting for 0.001 s. Time step for the integration is considered as 0.0001 s. Simply-supported boundary conditions are employed and all the four vertical

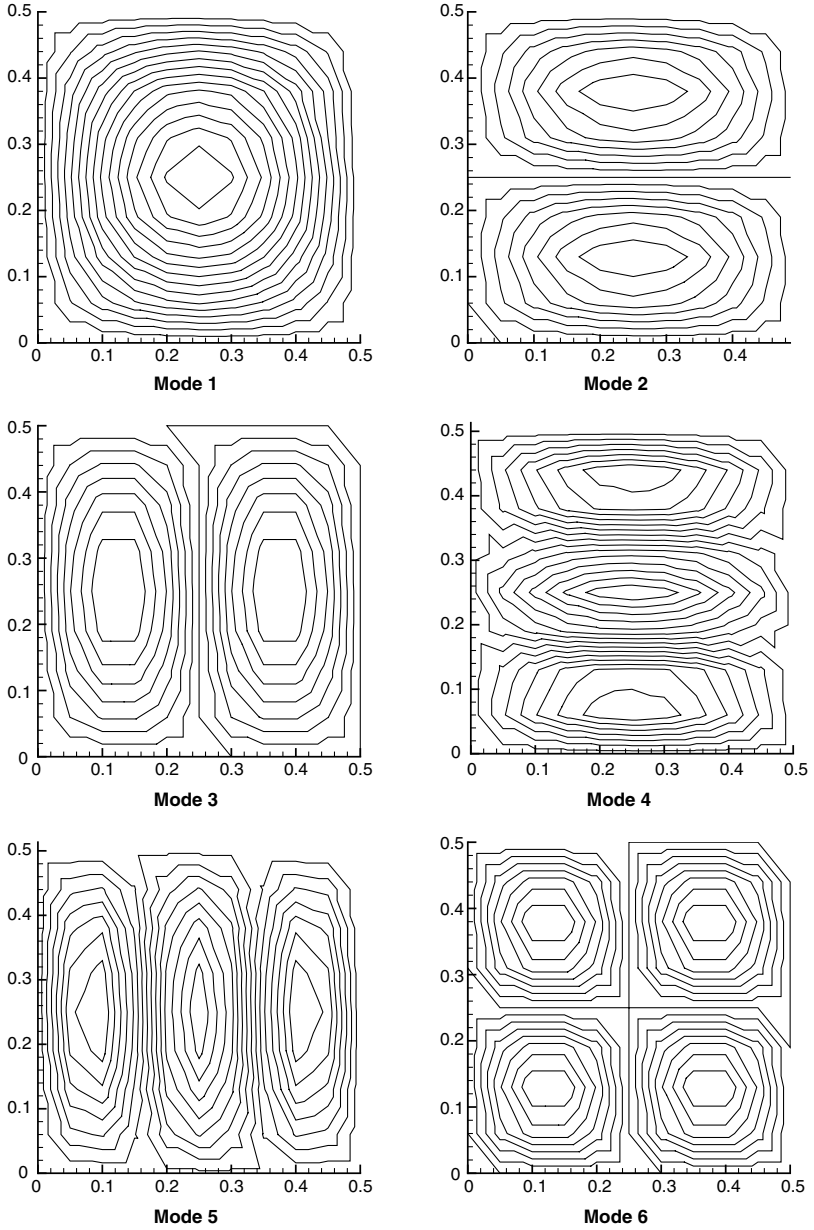

Fig. 11 Mode shapes of a [PZT/0/90/0/PZT] plate with length-to-thickness ratio of 50.

edges of the piezo is grounded. Further, the interface between the core and the piezo is grounded and electric potential ϕ_0 is applied on top and bottom surfaces of the plate as given Eq. (41). The response at the point $(0.5L_1/0.5L_2/0)$ is shown in Fig. 14. From the figure it can been seen that the effect of nonlinear stiffness terms is found to be negligible for this problem. The possible reason for this observation may be because the plate is moderately thick ($S = 50$) and hence the nonlinear effects seem to be small.

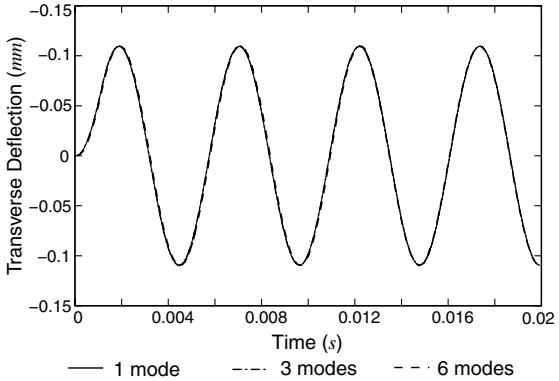

Fig. 12 Response at location $(0.5L_1/0.5L_2/0)$ of [PZT/0/90/0/PZT] plate subjected to an electric impulse load of 400 V/mm.

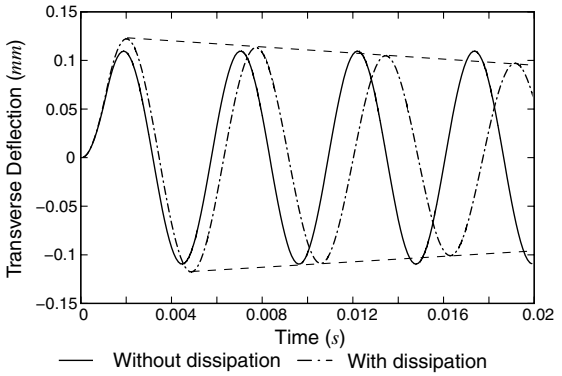

Fig. 13 Response at location $(0.5L_1/0.5L_2/0)$ of [PZT/0/90/0/PZT] plate subjected to an electric impulse load of 400 V/mm, with and without hysteresis dissipation.

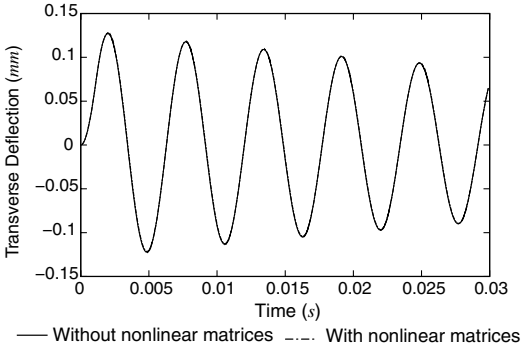

Fig. 14 Response at location $(0.5L_1/0.5L_2/0)$ of [PZT/0/90/0/PZT] plate with hysteresis dissipation and with and without nonlinear stiffness matrices, subjected to 400 V/mm impulse electric field.

VI. Conclusions

In this study, using the nonlinear electroelastic constitutive relations, variation of strain with respect to time varying electric field is analyzed, when the electric field is oscillated with varying amplitudes of electric field. When the amplitude of electric field is less than the coercive electric field corresponding to saturation polarization, the strain variation does not exhibit butterfly type loop. However, if the amplitude of the electric field is greater than the electric field corresponds to saturation polarization, strain variation exhibits a butterfly loop.

A layer-by-layer finite element formulation has been developed for static as well as dynamic analysis of smart structures including the hysteresis and nonlinear effects due to polarization–electric interaction. Using the finite element formulation, static linear and nonlinear analyses are carried out initially and validated with the experimental data given in the literature. It is observed from the results that the nonlinear formulation correlates better with the experimental data as compared with the linear case. In the case of transverse deflection, nonlinearity due to polarization–electric field interaction shows hardening effect, while for the longitudinal bending and twisting it shows softening effect.

In the dynamic analysis, polarization–electric field hysteresis effect introduces a friction-type damping. This study shows clearly that piezo layers can be used as effective dampers in addition to sensing and actuation of structures.

References

[1] Crawley, E. F., "Intelligent Structures for Aerospace: A Technological Overview and Assessment," *AIAA Journal*, Vol. 32, No. 8, 1994, pp. 1689–1699. doi:10.2514/3.12161

[2] Boller, C., "Monitoring the Integrity of Aircraft Structures: Current Procedures and Smart Sensing Options," *International Conference on Smart Materials, Structures and Systems*, Bangalore, India, 1999, pp. 31–43.

[3] Bossong, H., Lentzen, S., and Schmidt, R., "Experimental Investigation and Modeling of Piezoelectric Actuator Hysteresis for FE Analysis of Smart Structures," Indo-German Discussion Meeting on Smart Materials and Structures, IIT Kanpur, India, 2005.

[4] Toupin, R. A., "The Elastic Dielectrics," *Journal of Rational Mechanics and Analysis*, Vol. 5, No. 6, 1956, pp. 849–916.

[5] Tiersten, H. F., *Linear Piezoelectric Plate Vibration*, Plenum, New York, 1994.

[6] Tiersten, H. F., "On the Nonlinear Equations of Thermo-Electro-Elasticity," *International Journal of Engineering Science*, Vol. 9, 1971, pp. 587–604. doi:10.1016/0020-7225(71)90062-0

[7] Ahmad, S. N., Upadhyay, C. S., and Venkatesan, C., "Electro-thermo-elastic Formulation for the Analysis of Smart Structures," *Smart Materials and Structures*, Vol. 15, No. 2, 2006, pp. 401–416. doi:10.1088/0964-1726/15/2/021

[8] Wang, J., Shi, S. Q., Chen, L. Q., Li, Y., and Zhang, T. Y., "Phase Field Simulations of Ferroelectric/Ferroelastic Polarization Switching," *Acta Materialia*, Vol. 52, No. 3, 2004, pp. 749–764. doi:10.1016/j.actamat.2003.10.011

[9] Hwang, S. C., and McMeeking, R. M., "A Finite Element Model of Ferroelastic Polycrystals," *International Journal of Solids and Structures*, Vol. 36, No. 10, 1999, pp. 1541–1556. doi:10.1016/S0020-7683(98)00051-1

[10] Zhang, W., and Bhattacharya, K., "A Computational Model of Ferroelectric Domains. Part 1: Model Formulation and Domain Switching," *Acta Materialia*, Vol. 53, No. 1, 2005, pp. 185–198. doi:10.1016/j.actamat.2004.09.016

[11] Shaikh, M. G., Phanish, S., and Sivakumar, S. M., "Domain Switching Criteria for Ferroelectrics," *Journal of Computational Materials Science*, Vol. 37, Nos. 1–2, 2006, pp. 178–186. doi:10.1016/j.commatsci.2005.12.040

[12] Chen, P. J., and Montgomery, S. T., "A Macroscopic Theory for the Existence of the Hysteresis and Buttery Loop in Ferroelectricity," *Ferroelectrics*, Vol. 23, No. 2, 1980, pp. 199–208. doi:10.1080/00150198008018803

[13] Bassiouny, E., Ghaled, A. F., and Maugin, G. A., "Thermodynamical Formulation for Coupled Electromechanical Hysteresis Effects 1, Basic Equations, and 2, Poling of Ceramics," *International Journal of Engineering Science*, Vol. 26, No. 12, 1988, pp. 1279–1306. doi:10.1016/0020-7225(88)90047-X

[14] Bassiouny, E., Ghaleb, A. F., and Maugin, G. A., "Thermodynamical Formulation for Coupled Electromechanical Hysteresis Effects 3, Parameter Identification, and 4, Combined Electromechanical Loading," *International Journal of Engineering Science*, Vol. 27, No. 8, 1989, pp. 975–1000. doi:10.1016/0020-7225(89)90038-4

[15] Sateesh, V. L., Upadhyay, C. S., and Venkatesan, C., "Thermodynamic Modeling of Hysteresis Effects in Piezoceramics for Application to Smart Structures," *AIAA Journal*, Vol. 46, No. 1, 2008, pp. 280–284. doi:10.2514/1.31885

[16] Crawley, E. F., and Lazarus, K. B., "Induced Strain Actuation of Isotropic and Anisotropic Plates," *AIAA Journal*, Vol. 29, No. 6, 1991, pp. 944–951. doi:10.2514/3.10684

[17] Ray, M. C., Rao, K. M., and Samanta, B., "Exact Solution for Static Analysis of Intelligent Structures Under Cylindrical Bending," *Computers and Structures*, Vol. 47, No. 6, 1993, pp. 1031–1042. doi:10.1016/0045-7949(93)90307-Y

[18] Heyliger, P., and Brooks, S., "Exact Solutions for Laminated Piezoelectric Plates in Cylindrical Bending," *Journal of Applied Mechanics*, Vol. 63, No. 4, 1996, pp. 903–910. doi:10.1115/1.2787245

[19] Heyliger, P., "Static Behavior of Laminated Elastic/Piezoelectric Plates," *AIAA Journal*, Vol. 32, No. 12, 1994, pp. 2481–2484. doi:10.2514/3.12321

[20] Heyliger, P., "Exact Solution for Simply Supported Laminated Piezoelectric Plates," *Journal of Applied Mechanics*, Vol. 64, No. 2, 1997, pp. 299–306. doi:10.1115/1.2787307

[21] Vel, S. S., and Batra, R. C., "Exact Solution for Rectangular Sandwich Plates with Embedded Piezoelectric Shear Actuators," *AIAA Journal*, Vol. 39, No. 7, 2001, pp. 1363–1373. doi:10.2514/2.1455

[22] Vel, S. S., and Batra, R. C., "Three-Dimensional Analytical Solution for Hybrid Multilayered Piezoelectric Plates," *Journal of Applied Mechanics*, Vol. 67, No. 3, 2000, pp. 558–567. doi:10.1115/1.1311274

[23] Vel, S. S., and Batra, R. C., "Cylindrical Bending of Laminated Plates with Distributed and Segmented Piezoelectric Actuators/Sensors," *AIAA Journal*, Vol. 38, No. 5, 2000, pp. 857–867. doi:10.2514/2.1040

[24] Garcao, J. E. S., Soares, C. M. M., Soares, C. A. M., and Reddy, J. N., "Analysis of Laminated Adaptive Plate Structures Using Layerwise Finite Element Models," *Computers and Structures*, Vol. 82, Nos. 23–26, 2004, pp. 1939–1959. doi:10.1016/j.compstruc.2003.10.024

[25] Ha, S. K., Keilers, C., and Chang, F. K., "Finite Element Analysis of Composite Structures Containing Distributed Piezoceramic Sensors and Actuators," *AIAA Journal*, Vol. 30, No. 3, 1992, pp. 772–780. doi:10.2514/3.10984

[26] Saravanos, D. A., Heyliger, P. R., and Hopkins, D. A., "Layerwise Mechanics and Finite Element for the Dynamic Analysis of Piezoelectric Composite Plates," *International Journal of Solids and Structures*, Vol. 34, No. 3, 1997, pp. 359–378. doi:10.1016/S0020-7683(96)00012-1

[27] Jin, J., and Batra, R. C., "Effect of Electromechanical Coupling on Static Deformations and Natural Frequencies," *IEEE Transactions on Ultrasonics, Ferroelectrics, and Frequency Control*, Vol. 52, No. 7,

2005, pp. 1079–1093.
doi:10.1109/TUFFC.2005.1503994

[28] Heyliger, P., and Saravanos, D. A., "Exact Free-Vibration Analysis of Laminated Plates with Embedded Piezoelectric Layers," *Journal of the Acoustical Society of America*, Vol. 98, No. 3, 1995, pp. 1547–1557.
doi:10.1121/1.413420

[29] Kim, J., Varadan, V. V., and Varadan, V. K., "Finite-Element Modeling of a Smart Cantilever Plate and Comparison with Experiments," *Smart Materials and Structures*, Vol. 5, No. 2, 1996, pp. 165–170.
doi:10.1088/0964-1726/5/2/005

[30] David, C. O., and Touratier, M., "Multilayered Piezoelectric Refined Plate Theory," *AIAA Journal*, Vol. 41, No. 1, 2003, pp. 90–99.
doi:10.2514/2.1917

[31] Ahmad, S. N., Upadhyay, C. S., and Venkatesan, C., "Linear and Nonlinear Analysis of a Smart Beam Using General Electro-thermoelastic Formulation," *AIAA Journal*, Vol. 42, No. 4, 2004, pp. 840–848.
doi:10.2514/1.611

[32] Sateesh, V. L., Upadhyay, C. S., and Venkatesan, C., "Thermodynamic Modeling of Hysteresis Effects in Piezoceramics for Application to Smart Structures," *Proceedings of the 15th AIAA/ASME/AHS Adaptive Structures Conference*, AIAA Paper No. 2007-1743, Reston, VA, 2007.

[33] Mohite, P. M., and Upadhyay, C. S., "Accurate Computation of Critical Local Quantities in Composite Laminate Plates Under Transverse Loading," *Computers and Structures*, Vol. 84, Nos. 10–11, 2006, pp. 657–675.
doi:10.1016/j.compstruc.2005.11.004

[34] Kamlah, M., "Ferroelectric and Ferroelastic Piezoceramics Modeling of Electromechanical Hysteresis Phenomena," *Continuum Mechanics and Thermodynamics*, Vol. 13, No. 4, 2001, pp. 219–269.
doi:10.1007/s001610100052

F. Pai
Associate Editor